Lasers Med Sci (2016) 31:221–227
DOI 10.1007/s10103-015-1847-x

ORIGINAL ARTICLE

Photothermal cancer therapy by gold-ferrite nanocomposite and near-infrared laser in animal model

M. Heidari[1,2] · N. Sattarahmady[1] · N. Azarpira[3] · H. Heli[2] · A. R. Mehdizadeh[1] · T. Zare[1,2]

Received: 10 April 2015 / Accepted: 30 November 2015 / Published online: 22 December 2015

Abstract Surface plasmon resonance effect of gold nanostructures makes them good candidates for photothermal therapy (PTT) application. Herein, gold-ferrite nanocomposite (GFNC) was synthesized and characterized as a photothermal agent in PTT. The aim of this study was to investigate the effect of GFNC upon laser irradiation on treatment of cancer in mice bearing melanoma cancer. Thirty mice received 1.5×10^6 B16/F10 cells subcutaneously. After 1 week, the mice bearing solid tumor were divided into four groups: control group (without any treatment), laser group (received laser irradiation without GFNC injection), GFNC group (only received intratumorally GFNC), and GFNC+laser group (received intratumorally GFNC upon laser irradiation). In GFNC+laser group, 200 μL of fluid, 1.3×10^{-7} mol L^{-1} gold nanoparticles, was injected intratumorally and immediately the site of tumor was exposed to continuous wave diode laser beam (808 nm, 1.6 W cm^{-2}) for 15 min. All mice but four were euthanized 24 h after treatment to compare the necrotic surface area histologically by using measuring graticule. Statistical analyses revealed significant differences in necrosis extent for GFNC+laser group, compared to other groups. Four subjects (control group and GFNC+laser group, two mice each) were kept for longitudinal study. Histological analyses and tumor volume measurements of the four subjects indicated that tumor in GFNC+laser group was controlled appropriately. It was concluded that combining an 808-nm laser at a power density of 1.6 W cm^{-2} with GFNC has a destruction effect in melanoma cancer cells in an animal model.

Keywords Photothermal therapy · Melanoma cancer · Diode laser · Gold-ferrite nanocomposite

Introduction

Today, there is high demand to replace conventional therapeutic strategies with non-invasive methods for cancer treatment. The aims of these new methods are to diagnosis cancer early, preserve normal tissues, and decrease side effects [1, 2]. Using different sources of energy is a base for these new methods, such as ultrasound, microwave, radiofrequency, cold, heat, and light [3]. Therapeutic approaches based on using light include photodynamic therapy (PDT) and photothermal therapy (PTT). PDT is a light-activated method of photosensitizers to generate reactive oxygen species. PTT is tissue ablation via photothermal effect of a light source [4, 5]. Generally, for minimizing radiant absorption in hemoglobin and water as major absorbers of light in the body, to reach deeper penetration of radiant in tissue, near-infrared (NIR) wavelengths around 650–900 nm are used [6]. Studies [7, 8] showed temperature increment by laser irradiation between 42 and 60 °C will develop coagulative necrosis in 24 to 72 h after treatment.

Metal nanoparticles (NPs) such as gold nanostructures [9–12] and carbon nanostructures [13, 14] absorb light and act as photothermal agents and, therefore, improve the

✉ N. Sattarahmady
nsattar@sums.ac.ir; sattarahmady@yahoo.com

[1] Department of Medical Physics, School of Medicine, Shiraz University of Medical Sciences, Shiraz, Iran

[2] Nanomedicine and Nanobiology Research Center, Shiraz University of Medical Sciences, Shiraz, Iran

[3] Transplant Research Center, Shiraz University of Medical Sciences, Shiraz, Iran

efficiency of NIR penetration depth. Also, visible light excitation of metal NPs induces singlet O_2 formation and PDT [15]. Among all metallic nanostructures, gold nanostructures are exclusive with remarkable optical properties due to size confinement and surface plasmon resonance (SPR) effects. The frequency of the SPR relies on the size, shape, and dielectric properties of the particles, and gold nanostructures possess adjustable optical properties [16].

In the field of theranostic nanomedicine, multifunctional nanomaterials that combine several abilities are simultaneously employed for diagnosis, follow-up, and treatment of tumors [17, 18]. Gold NP-based multifunctional nanocomposites [19] and carbon nanotube-based nanocomposites [20], like gold/single wall carbon nanotubes [21], are among theranostic agents which employ optical properties of gold nanostructures. Spinel ferrite NPs, with general formula MFe_2O_4, M= Ni^{2+}, Mn^{2+}, Zn^{2+}, or Co^{2+}, have potential applications for magnetic resonance imaging, cell labeling, drug delivery, and hyperthermia [22]. By combination of magnetic properties of magnetic materials and plasmonic properties of other NPs, theranostic approaches with further therapeutic and diagnostic modalities would be provided [23]. For this purpose, a variety of nanocomposites have been designed. One example is the nanocomposites of iron oxides NPs and cancer-targeting materials [24]. In another study [25], Fe_3O_4/Au nanocomposite was synthesized to make a multifunctional material with both magnetic and optical properties.

To achieve multimodal imaging, MRI and fluorescence imaging, as well as photothermal ablation, gold nanoshell-based complexes [17], or other composites of gold nanostructures with magnetic materials are among the best candidates.

In the present study, gold-ferrite nanocomposite (GFNC) as a single composite nanomaterial that can be used in various therapeutic modalities was synthesized and characterized by transmission electron microscopy (TEM), Fourier transform infrared spectroscopy (FTIR), and UV-vis spectrophotometry. GFNC was exposed to a continuous-wave (CW) diode laser at 808 nm to assess photothermal effect of the nanostructure. Finally, ablation of cancer cells by using this effect was explored in mice bearing implanted melanoma tumor. In this regard, soon after intratumorally injection of GFNC, tumor site exposed to the laser beam, and after 24 h, histological analyses were performed.

Materials and methods

Materials

All chemicals were used without further purification and obtained from Sigma Chemicals Co. (USA), Scharlau Chemie Co. (Spain), or Merck Co. (Germany). Dextrin was obtained by roasting pure corn starch at 200 °C for 2 h.

Synthesis and characterization of CFNPs and GFNC

Dextrin-coated $Co_{0.5}Zn_{0.5}Fe_2O_4$ NPs (CFNPs) were synthesized by the aqueous precipitation technique. Briefly, the individual metal chloride, in the appropriate stoichiometric proportions (mole ratio of Co/Zn/Fe of 0.5/0.5/2), was dissolved in a diluted HCl solution (0.1 mol L^{-1}) and was heated to 80 °C. A 4 mol L^{-1} NaOH and 12.5 g dextrin were prepared separately and heated to 80 °C. These hot solutions were then rapidly mixed with stirring (final pH of 12.0). The temperature was then increased to 100 °C and stirring was continued for 1 h, for crystallization of the ferrites. Then, the solution was cooled and the precipitate was collected by a permanent magnet and washed several times with distilled water to neutralize the supernatant.

Synthesized dextrin-coated CFNPs (100 μL of 0.1 mg μL^{-1}) were transferred to a vortexing solution of 100 mL of deionized water containing 0.16 g $HAuCl_4$. After heating the mixture to its boiling point, 400 μL heat solution of 0.1 M sodium citrate was added immediately and was stirred for 1 h until a clear pinkish solution of GFNC was formed.

UV-vis spectroscopy of CFNPs and GFNC were recorded on a Rayleigh UV2601 double beam UV-vis spectrophotometer. The size of GFNC was characterized by using Zeiss-EM10C transmission electron microscope operating at 80 kV, on a carbon formvar-coated copper grid. FTIR was performed by Burker Tensor 27 to identify surface structure of the sample.

Photothermal effect in GFNC solutions upon laser irradiation

An 808-nm diode laser was applied as a light source with a lens mounting at the output that allowed the laser spot size to be changed by changing the distance from the output to the target. The output power was independently calibrated by using a handheld optical power meter (Lambda, Australia) and was found to be 1.0 W for a spot in diameter of 3.5 mm (~8 W cm^{-2}) and a 2-A supply current. Laser light with an output power density of 1.6 W cm^{-2} was focused separately into two 1.5-mL autoclavable plastic vials, containing 900 μL of GFNC. The concentrations of gold NPs (GNPs) in the samples were 6.65×10^{-9} and 1.3×10^{-7} mol L^{-1} obtained by measuring their absorbance and using an absorption coefficient of 1.89×10^{8} mol^{-1} L^{-1} cm^{-1} (for 12-nm GNPs).

The temperature changes in GFNC fluid during laser irradiation were measured by a thermoprobe (DAJ Co., Iran) over a period of 10 min. The probe was placed vertically in the center of the samples, approximately 3–5 mm deep inside the vials. Water was used as a control sample in the same conditions.

Cell and mice preparations

Mouse malignant melanoma cell line C540 (B16/F10) was obtained from National Cell bank of Iran (NCBI) affiliated to Pasteur Institute of Iran (http://ncbi.pasteur.ac.ir/). The cells were cultured in RPMI medium with 10 % fetal bovine serum and 1 % penicillin-streptomycin in a humidified cell culture incubator at 37 °C, 5 % CO_2.

Thirty male BALB/c mice (5 weeks old, body weight of ~20 g) were obtained from the center of comparative and experimental medicine, Shiraz, Iran. The protocol was approved by the committee on the Ethics of Animal Experiments of Shiraz University of Medical Sciences. The animals were housed in special cages at a controlled temperature (24±2 °C) and humidity (40–70 %) with weekly floor exchange. They had free access to water and standard pelleted laboratory animal diets. A 12:12 light/dark cycle was followed in the mentioned animal vivarium.

Tumor implantation and NIR laser irradiation of tumor in mice

The tumors were implanted by subcutaneous injection of 1.5×10^6 B16/F10 cells in 100 μL phosphate buffer saline into the back of the neck of male BALB/c mice. Approximately, 1 week after tumor implantation, solid tumors appeared. Twenty-three mice bearing implanted tumors with the average tumor volume of about 0.55 cm^3 were selected for treatment and were randomly divided into four groups. During the treatment process, all subjects were anesthetized with intramuscular injection mixture of ketamin (10 %) and xylazine (2 %) and the subjects were shaved in the tumor areas.

Four animal groups include the control group (six tumor-bearing mice with no treatment), laser group (six tumor-bearing mice received intratumorally injection of saline and laser irradiation), GFNC group (three tumor-bearing mice only received intratumorally GFNC injection), and GFNC+laser group (eight tumor-bearing mice received GFNC fluid and laser irradiation). GFNC fluid (the concentration of GNPs was 1.3×10^{-7} mol L^{-1}) was injected intratumorally to the subjects of GFNC and GFNC+laser groups correspond to a dosage of 2.7×10^{-11} mol $mice^{-1}$ GNPs. Slow injection of the fluid in two locations of the tumors was tried (with a rate of injection of ~15 μL s^{-1}) to have a good distribution of GFNC in the tumors. Immediately after injections, tumor site of the subjects in laser group and GFNC+laser group was exposed to a CW diode laser (808 nm; 1.0 W, DAJ Co., Iran) with a power density of 1.6 W cm^{-2} for 15 min. After 24 h, all subjects but four were sacrificed and the tumoral masses were removed.

To investigate the overall health condition of mice, their body weights were measured before the treatment and before the euthanasia. The four subjects (control group and GFNC+laser group, two mice each) were kept for longitudinal study to ensure health condition of mice for a longer period of time and weather GFNC particles had still remained in the tumor. Two subjects in the GFNC+laser group were followed for 2 weeks, but two of them in the control group were followed until the 8th day. Since their tumor volume was more than 800 mm^3, they were sacrificed due to ethics. During this time, subjects were monitored by tumor size measuring via a caliper and body weight measurements. After this time, their tumors and tissues of the liver, kidney, and spleen were removed for histological analyses.

Histological analyses of tumor tissues

The removed tumor tissues were fixed in 10 % buffered formalin, routinely processed, and embedded in paraffin. Sections with 3–5 μm were prepared and analyzed after hematoxylin and eosin (H&E) and Pearl's iron staining. The Pearl's iron stain was used to confirm the presence of NPs and to differentiate NPs from melanin pigments which were produced by tumoral cells. After preparation of slides from tumor tissues, the inflammation and necrotic surface area were estimated by using measuring graticule (Olympus, Japan) in subjects of four groups. The percentage of necrosis (with a ×400 magnification) against the whole tumor area was estimated and graded; 100, 75, 50, 25, 12.5 %, and no necrosis. These were considered as 5^+, 4^+, 3^+, 2^+, 1^+, and zero, correspondingly [26]. In order to investigate the severity of inflammation based on the presence of acute and chronic inflammatory, all infiltration was graded as sever (5^+), moderate (4^+), mild (3^+), few (2^+), and no (0). Finally, the data corresponding to necrosis and inflammation grading in all subjects, as non-parametric data, was analyzed statistically via the Kruskal-Wallis test (SPSS version 15) to investigate significant differences (at a level of 5 %) in necrosis and inflammation extent among four groups. The Mann-Whitney test was performed to investigate pair-wise comparison.

Results and discussion

Over the past several decades, melanoma incidence has almost reached epidemic proportion. Late-stage melanoma is not curable by current clinical tools [27, 28]. Therefore, hyperthermia as a comprehensive treatment has potential to ablate this type of cancer. For this purpose, GFNC was synthesized and characterized by TEM, FTIR, and UV-vis spectrophotometry.

A TEM image of GFNC is shown in Fig. 1a. It clearly shows that the synthesized GFNC is a mixture of spherical structure of $Zn_{0.5}Co_{0.5}Fe_2O_4$ NPs (FCNPs) with the mean diameter of 4 nm and GNPs with the mean diameter of 12 nm with higher contrast. Figure 1b shows the UV-vis absorption spectra of GFNC. The maximum absorption of

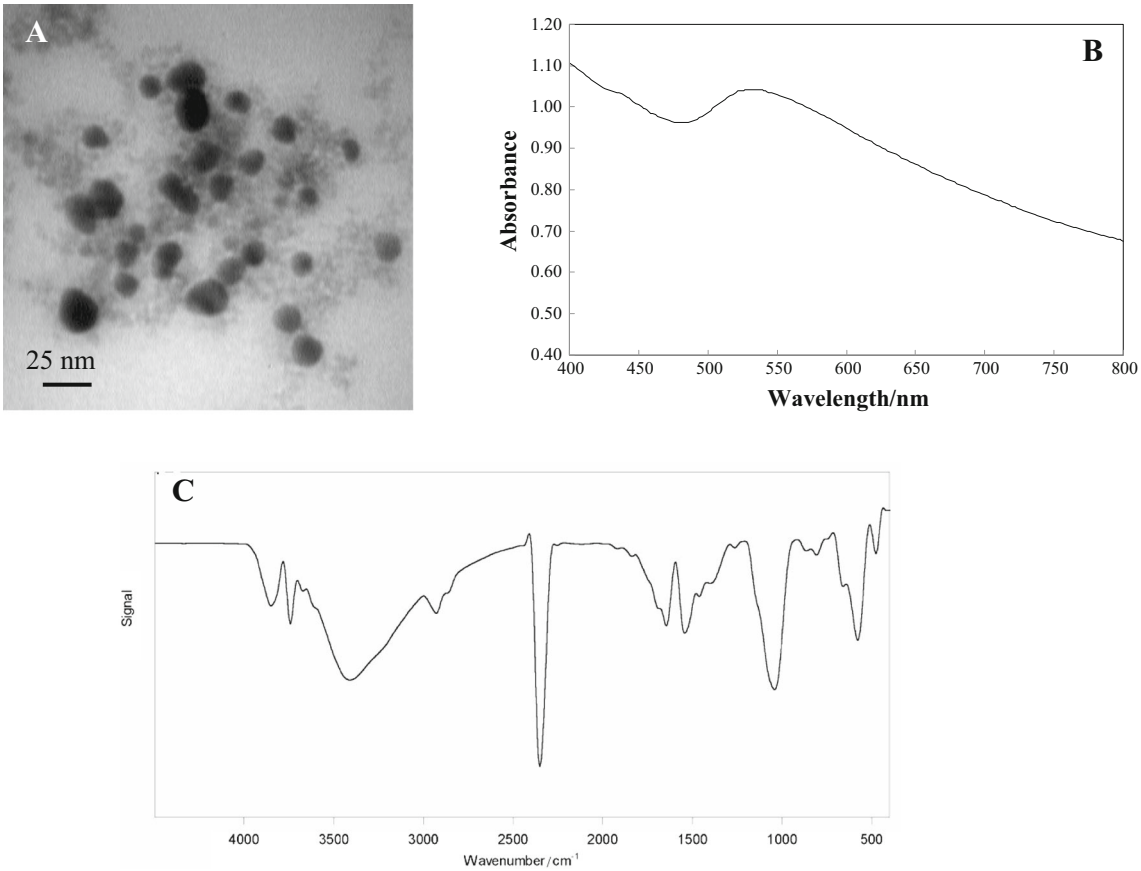

Fig. 1 **a** TEM image of GFNC, particles with higher contrast are GNPs and others are $Co_{0.5}Zn_{0.5}Fe_2O_4$ NPs. **b** UV-vis absorption spectra of GFNC. **c** FTIR spectra of GFNC

GFNC is about 530 nm based on SPR of GNPs. A FTIR spectrum of FCNPs is shown in Fig. 1c. In the spectrum, bands at around 3420, 2924, and 1045 cm^{-1} were related to O–H stretching vibration, the symmetric vibration of $–CH_2–$ group, and the –CO– vibration of the alcohol functional group. These results confirmed surface coating FCNPs by a dextrin layer.

To evaluate the photothermal effect of GFNC, the temperature enhancement of two different concentrations of GFNC was measured under NIR irradiation (808 nm) at a power density of 1.6 W cm^{-2} during 10 min. The temperature increments in the control sample and GFNC fluids with concentrations of 6.5×10^{-10} and 1.3×10^{-7} mol L^{-1} GNPs after 10 min of laser exposure were 10.3, 18.5, and 25.8, respectively (Fig. 2). The temperature increment is concentration dependent, and both concentrations exhibited a very intense photothermal effect under NIR irradiation, compared to the control sample. GFNC with the concentration of 1.3×10^{-7} mol L^{-1} GNPs showed a maximum temperature of 54.8 °C. Therefore, GFNC at the concentration of 1.3×10^{-7} mol L^{-1} GNPs under the 808-nm laser irradiation was selected for in vivo studies.

After the treatment process, for histologically evaluating the PTT-mediated efficiency on the destruction of malignant cells in four subject groups, animals were sacrificed 24 h after treatment. Both treated and non-treated tumors were composed of one nodule that contains malignant melanoma cells with melanin pigments. After Pearl's iron staining, it was found that GFNC is in black color and melanin pigment is in brown color in H&E-stained images. Figure 3a shows the microscopy image of a Pearl's iron-stained slide of a tumor which indicates the presence of iron particles near tumoral

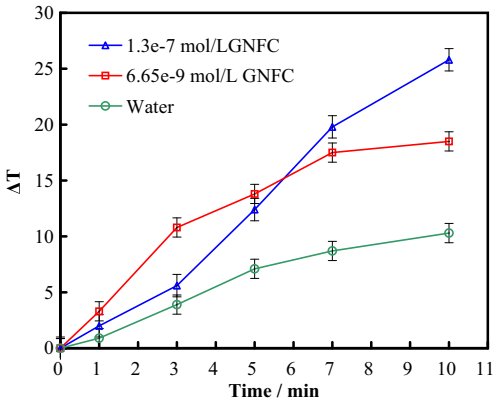

Fig. 2 The temperature increases for GFNC with concentrations of 1.3×10^{-7} mol L^{-1} (*circle*), 6.65×10^{-9} (*square*), and control sample (*triangle*) exposed to an 808-nm diode laser irradiation during 10 min

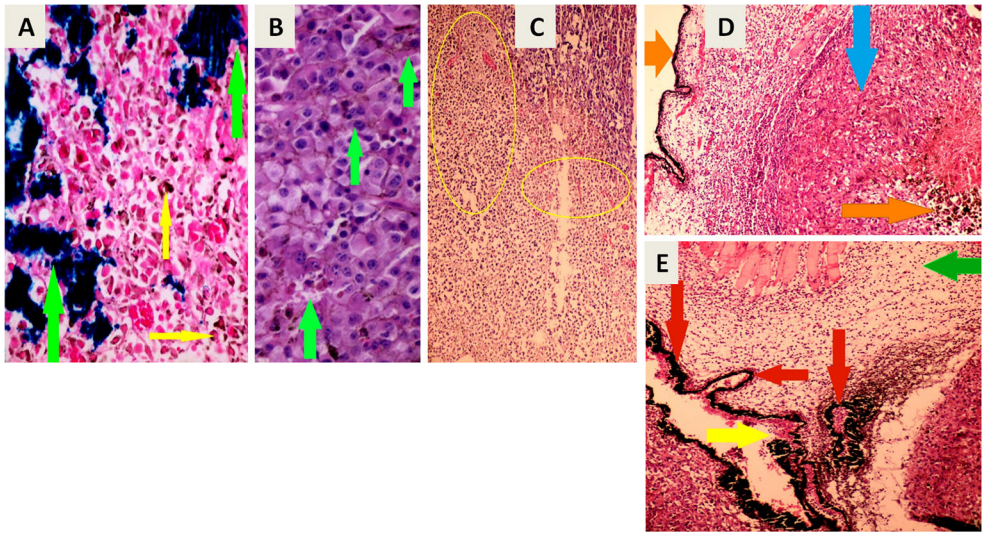

Fig. 3 **a** Image of Pearl's iron staining for detection of NPs. Iron particles in GFNC are stained as blue (*green arrows*). The melanin pigment is seen as brownish pigment in malignant cells (*yellow arrows*). **b** Images of H&E-stained slides (×400) of non-treated tumor with viable malignant cells containing brownish melanin pigment (*green arrows*). **c** H&E-stained slide (×400) of the subject in the laser group with intermediate necrosis level. **d** The GFNC group. The GFNC particles are easily seen as black dot areas near tumor cells (*orange arrows*). Viable malignant cells are seen (*blue arrow*), too. No necrosis is observed around GFNC. **e** H&E-stained slide (×400) of the subject in the GFNC+laser group. *Yellow*, *green*, and *orange arrows* show coagulative necrosis, inflammation, and GFNC, respectively

cells. Figure 3b–e shows microscopy images of H&E-stained tumor slides of the four groups. Figure 3b shows viable malignant cells in tumoral tissue (grade 1 necrosis). Figure 3c shows foci of coagulative tumor cell necrosis (grade 3 necrosis) in the subjects of laser group. Figure 3d shows no necrosis in surrounding area of the NPs in H&E-stained slides of the GFNC group (grade 1 necrosis). Therefore, treatment of tumor with GFNC in the absence of laser irradiation does not cause any anti-melanoma effect on tumoral cells. Tumors of GFNC+laser group show more severe coagulative necrosis around the tumors as well as the centers of tumors in comparison to tumors in other groups. Abundant iron particles were present as both extracellular (in tumor cells) and intracellular (intracytoplasmic) in tumor centers of groups received GFNC injection (Fig. 3d, e).

In GFNC+laser group, a large amount of cancer cells was destroyed due to photothermal therapy (grade 5 necrosis). As shown in Fig. 3e, necrotic areas were around the NPs which prove the effect of heat dissipation due to the presence of GNPs under laser irradiation.

Statistically, it was indicated that there were significant differences between the four groups in necrosis area (p value=0.006, statistical value=17.602) and the Mann-Whitney test showed significant differences between GFNC+laser group with other groups in necrosis extent (p values<0.05). All groups revealed variable degrees of inflammation surrounding tumor walls, but differences were not statistically significant (p value=0.125, statistical value=5.741).

The treatment was also evaluated after 2 weeks from the treatment in GFNC+laser group compared to control group with monitoring of the tumor volume (Fig. 4) and histological analyses (Fig. 5). Figure 4 shows tumor volume in control subjects had a rapid upward trend while tumor growth in GFNC+laser group was controlled appropriately. Figure 5a illustrates H&E-stained images of the subject in GFNC+laser group. As it can be seen in this figure, cancer cells are thermally ablated while the melanin pigments are present. Plenty of black spots can be seen in these images attributed to the presence of GFNC. Figure 5b–d indicates that no particle is evident in organs like the kidney, spleen, and liver and they have normal tissues. Absence of NPs in these organs in subjects euthanized 24 h after treatment as well as subjects of the longitudinal study is related to particles size and intratumoral administration of them. It was reported that particles with a diameter more than 50 nm are taken up by the liver after

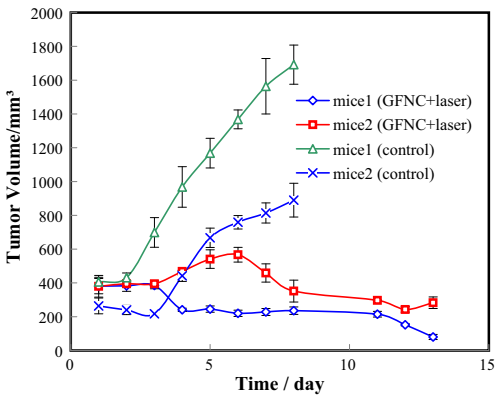

Fig. 4 Tumor volume changes vs. days after treatment in the longitudinal study for two mice in the GFNC+laser group (*triangle*, *multiplication sign*) and two mice in the control group (*diamond*, *square*), during 2 weeks

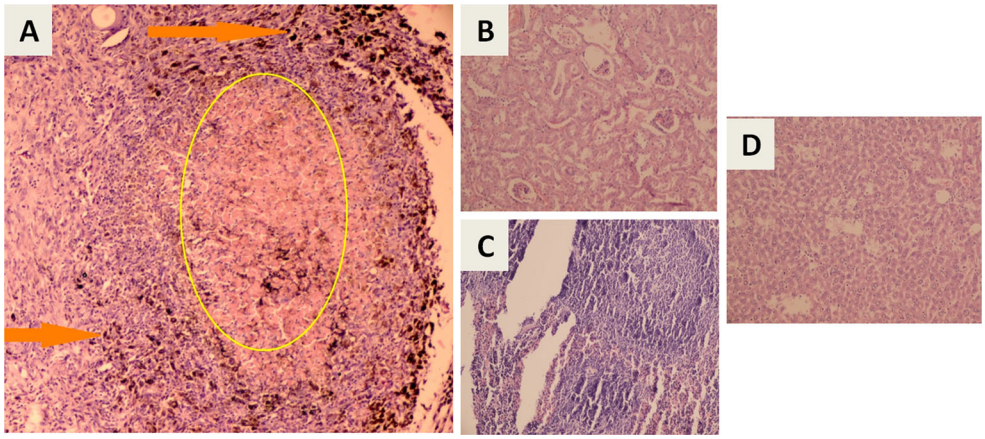

Fig. 5 **a** H&E-stained slide of tumor of subject in the GFNC+laser group of the longitudinal study after 2 weeks. *Yellow border* and *orange arrows* show necrosis area and GFNC, respectively. **b** H&E-stained slide (×400) of normal kidney of a subject who received GFNC+laser. **c** H&E-stained slide (×400) of normal spleen of subject received GFNC+laser. **d** H&E-stained slide (×400) of normal liver of subject received GFNC+laser

intravenous injection [29]. It should be noted that no loss in mice body weight was observed. Therefore, the photothermal therapy did not have negative influence on overall health of mice after the treatment until 2 weeks.

Other thermal ablation approaches using radiofrequency and microwave did not induce adequate heating and it damaged healthy tissues [30–34]; however, results show gold nanostructures accompanied by laser irradiation have potential to destroy tumor cells without damaging the surrounding healthy tissues. With the limitation of this study, the groups with laser irradiation show a degree of surface ulceration, so in the future study, tailored nanostructures with shorter laser irradiation time help to remove this side effect. Because GFNC is a composite of GNPs and magnetic NPs, FCNPs, it has potential to be used as a multifunctional agent which enables multimodal imaging (MRI and NIR fluorescence imaging) and therapy [17]. In addition, while the depth penetration of NIR laser was 0.5 cm, using internal fiber optic laser source for treating tumors in the body can be useful [35].

Conclusions

In this study, we present that GFNC is a good NIR light-activatable photothermal therapy agent. Photothermal outcome due to these NPs depends on their concentration and power density of laser irradiation. GFNC enabled to destroy B16F0 melanoma tumors in mice upon NIR light irradiation (via an 808-nm diode laser) without additional organic photosensitizers. Results show necrosis area in the GFNC+laser group compared to other groups was statistically the largest, with a p value of 0.006 and statistical value of 17.602, but inflammation severity in all groups was not statistically different with p value and statistical value of 0.125 and 5.741, respectively. After 2-week monitoring tumor volumes of the mice received GFNC+laser, it was illustrated that after treatment, the mice were in good health condition and the malignant cells were ablated suitably. Therefore, PTT-mediated GFNC with a minimum invasive therapeutic method might be effective in destroying tumor cells, and after some modifications, it might be used clinically.

Acknowledgments We would like to thank the Research Councils of Shiraz University of Medical Sciences (7803) for supporting this research and the Research Consultation Center, Shiraz University of Medical Sciences. The authors would also like to acknowledge Mr. Kouhi, Mr. Dideban-Mehr, and Mrs. Esfandiari for their efforts.

Compliance with ethical standards

Conflict of interest The authors declare that they have no competing interests.

Ethics approval This study was conducted according to the Committee on the Ethics of Animal Experiments of Shiraz University of Medical Sciences.

References

1. Ji Z, Lin G, Lu Q et al (2012) Targeted therapy of SMMC-7721 liver cancer in vitro and in vivo with carbon nanotubes based drug delivery system. J Colloid Interface Sci 365(1):143–149. doi:10.1016/j.jcis.2011.09.013
2. Alexis F, Rhee JW, Richie JP et al (2008) New frontiers in nanotechnology for cancer treatment. Urol Oncol 26(1):74–85. doi:10.1016/j.urolonc.2007.03.017
3. Betrouni N, Colin P, Bozzini G et al (2013) Image-guided laser therapies for prostate cancer. IRBM 34:28–32. doi:10.1016/j.irbm.2012.12.006
4. Huang X, El-Sayed MA (2011) Plasmonic photo-thermal therapy (PPTT). Alex J Med 47:1–9. doi:10.1016/j.ajme.2011.01.001
5. Master A, Livingston M, Sen Gupta A (2013) Photodynamic nanomedicine in the treatment of solid tumors: perspectives and

challenges. J Control Release 168(1):88–102. doi:10.1016/j.jconrel.2013.02.020
6. Weissleder R (2001) A clearer vision for in vivo imaging. Nat Biotechnol 19(4):316–317
7. Colin P, Nevoux P, Marqa M et al (2012) Focal laser interstitial thermotherapy (LITT) at 980 nm for prostate cancer: treatment feasibility in Dunning R3327-AT2 rat prostate tumour. BJU Int 109(3):452–458. doi:10.1111/j.1464-410X.2011.10406.x
8. van Nimwegen SA, L'Eplattenier HF, Rem AI et al (2009) Nd:YAG surgical laser effects in canine prostate tissue: temperature and damage distribution. Phys Med Biol 54(1):29–44. doi:10.1088/0031-9155/54/1/003
9. Sassaroli E, Li KCP, O'Neill BE (2009) Numerical investigation of heating of a gold nanoparticle and the surrounding microenvironment by nanosecond laser pulses for nanomedicine applications. Phys Med Biol 54:5541–5560. doi:10.1088/0031-9155/54/18/013
10. Huang X, Jain P, El-Sayed I et al (2008) Plasmonic photothermal therapy (PPTT) using gold nanoparticles. Lasers Med Sci 23:217–228. doi:10.1007/s10103-007-0470-x
11. O'Neal DP, Hirsch LR, Halas NJ et al (2004) Photo-thermal tumor ablation in mice using near infrared-absorbing nanoparticles. Cancer Lett 209:171–176
12. Terentyuk GS, Maslyakova GN, Suleymanova LV et al (2009) Laser-induced tissue hyperthermia mediated by gold nanoparticles: toward cancer phototherapy. J Biomed Opt 14:021016. doi:10.1117/1.3122371
13. Xiao Y, Gao X, Taratula O et al (2009) Anti-HER2 IgY antibody-functionalized single-walled carbon nanotubes for detection and selective destruction of breast cancer cells. BMC Cancer 9:351. doi:10.1186/1471-2407-9-351
14. Zhou F, Xing D, Ou Z et al (2009) Cancer photothermal therapy in the near-infrared region by using single-walled carbon nanotubes. J Biomed Opt 14:021009. doi:10.1117/1.3078803
15. Cheng Y, Meyers JD, Broome AM et al (2011) Deep penetration of a PDT drug into tumors by noncovalent drug-gold nanoparticle conjugates. J Am Chem Soc 133:2583–2591
16. Zeng S, Yong KT, Roy I (2011) A review on functionalized gold nanoparticles for biosensing applications. Plasmonics 6:491–506. doi:10.1007/s11468-011-9228-1
17. Bardhan R, Lal S, Joshi A et al (2011) Theranostic nanoshells: from probe design to imaging and treatment of cancer. Acc Chem Res 44(10):936–946. doi:10.1021/ar200023x
18. Khlebtsov N, Bogatyrev V, Dykman L et al (2013) Analytical and theranostic applications of gold nanoparticles and multifunctional nanocomposites. Theranostics 3(3):167–180. doi:10.7150/thno.5716
19. Khlebtsov B, Panfilova E, Khanadeev V et al (2011) Nanocomposites containing silica-coated gold-silver nanocages and Yb-2, 4-dimethoxyhematoporphyrin: multifunctional capability of IR-luminescence detection, photosensitization, and photothermolysis. ACS Nano 5:7077–7089. doi:10.1021/nn2017974
20. Chen YC, Huang XC, Luo YL et al (2013) Non-metallic nanomaterials in cancer theranostics: a review of silica- and carbon-based drug delivery systems. Sci Technol Adv Mater 14:1–23. doi:10.1088/1468-6996/14/4/044407
21. Kim JW, Galanzha EI, Shashkov EV et al (2009) Golden carbon nanotubes as multimodal photoacoustic and photothermal high-contrast molecular agents. Nat Nanotechnol 4(10):688–694. doi:10.1038/nnano.2009.231
22. Ahamed M, Akhtar MJ, Siddiqui MA et al (2011) Oxidative stress mediated apoptosis induced by nickel ferrite in cultured A549 cells. Toxicology 283(2–3):101–108. doi:10.1016/j.tox.2011.02.010
23. Wu CH, Sokolov K (2014) Synthesis of immunotargeted magneto-plasmonic nanoclusters. J Vis Exp (90). doi: 10.3791/52090
24. Yu MK, Park J, Jon S (2012) Targeting strategies for multifunctional nanoparticles in cancer imaging and therapy. Theranostics 2:3–34
25. Lin FH, Doong RA (2010) Synthesis of ferrite nanoparticle and ferrite-gold heterostructures. Adv Mater Res 123–125:251–255. doi:10.4028/www.scientific.net/AMR.123-125.251
26. Melancon MP, Elliott A, Ji X et al (2011) Theranostics with multifunctional magnetic gold nanoshells: photothermal therapy and t2* magnetic resonance imaging. Investig Radiol 46(2):132–140. doi:10.1097/RLI.0b013e3181f8e7d8
27. Balivada S, Rachakatla RS, Wang H et al (2010) A/C magnetic hyperthermia of melanoma mediated by iron(0)/iron oxide core/shell magnetic nanoparticles: a mouse study. BMC Cancer 10:119–127. doi:10.1186/1471-2407-10-119
28. Glusac EJ (2012) The melanoma 'epidemic', a dermatopathologist's perspective. J Cutan Pathol 39(1):17–20. doi:10.1111/j.1600-0560.2010.01660.x
29. Abdeen S, Praseetha PK (2013) Diagnostics and treatment of metastatic cancers with magnetic nanoparticles. J Nanomedine Biotherapeutic Discov 3:115. doi:10.4172/2155-983X.1000115
30. Edrei Y, Gross E, Corchia N et al (2011) Vascular profile characterization of liver tumors by magnetic resonance imaging using hemodynamic response imaging in mice. Neoplasia 13(3):244–253
31. Lencioni R, Cioni D, Crocetti L et al (2005) Early-stage hepatocellular carcinoma in patients with cirrhosis: long-term results of percutaneous image-guided radiofrequency ablation. Radiology 234(3):961–967
32. Lau WY, Lai EC (2009) The current role of radiofrequency ablation in the management of hepatocellular carcinoma: a systematic review. Ann Surg 249(1):20–25. doi:10.1097/SLA.0b013e31818eec29
33. Liang P, Dong B, Yu X et al (2005) Prognostic factors for survival in patients with hepatocellular carcinoma after percutaneous microwave ablation. Radiology 235(1):299–307
34. Hinshaw JL, Lee FT Jr (2007) Cryoablation for liver cancer. Tech Vasc Interv Radiol 10(1):47–57. doi:10.1053/j.tvir.2007.08.005
35. Robinson JT, Welsher K, Tabakman SM et al (2010) High performance in vivo near-IR (>1 μm) imaging and photothermal cancer therapy with carbon nanotubes. Nano Res 3(11):779–793. doi:10.1007/s12274-010